Structure and property evaluation of a vacuum plasma sprayed nanostructured tungsten-hafnium carbide bulk composite

Rea, K. E.; Viswanathan, V.; Kruize, A.; De Hosson, J. Th. M.; O'Dell, S.; McKechnie, T.; Rajagopalan, S.; Vaidyanathan, R.; Seal, S.; O'Dell, S.

Published in:
Materials science and engineering a-Structural materials properties microstructure and processing

DOI:
10.1016/j.msea.2007.05.063

Publication date:
2008

ELSEVIER

Materials Science and Engineering A 477 (2008) 350–357

MATERIALS SCIENCE & ENGINEERING A

www.elsevier.com/locate/msea

Structure and property evaluation of a vacuum plasma sprayed nanostructured tungsten–hafnium carbide bulk composite

K.E. Rea [a,b], V. Viswanathan [a,b], A. Kruize [a,b], J.Th.M. De Hosson [c], S. O'Dell [d], T. McKechnie [d], S. Rajagopalan [b], R. Vaidyanathan [b], S. Seal [a,b,*]

[a] *Surface Engineering and Nanotechnology Facility (SNF), University of Central Florida, Eng. 381, 4000 Central Florida Blvd., Orlando, FL 32816, United States*

[b] *AMPAC, Department of Mechanical, Materials, and Aerospace Engineering (MMAE), Nanoscience and Technology Center, University of Central Florida, Eng. 381, 4000 Central Florida Blvd., Orlando, FL 32816, United States*

[c] *Department of Applied Physics, University of Groningen, Nijenborgh 4, NL-9747 AG, Netherlands*

[d] *Plasma Processes, Inc., 4914 Moores Mill Road, Huntsville, AL 35811, United States*

Received 12 January 2007; received in revised form 10 May 2007; accepted 14 May 2007

Abstract

Vacuum plasma spray (VPS) forming of tungsten-based metal matrix nanocomposites (MMCs) has shown to be a cost effective and time saving method for the formation of bulk monolithic nanostructured thermo-mechanical components. Spray drying of powder feedstock appears to have a significant effect on the improved mechanical properties of the bulk nanocomposite. The reported elastic modulus of the nanocomposite nearly doubles due to the presence of HfC nano particulates in the W matrix. High resolution transmission electron microscopy (HRTEM) revealed the retention of nanostructures at the select process conditions and is correlated with the enhanced mechanical properties of the nanocomposite. Published by Elsevier B.V.

Keywords: Powder processing; Nanoindentation; Transmission electron microscopy; Carbides; Nanocomposites

1. Introduction

Nanostructured materials are widely researched for their mechanical, thermal, optical and electrical properties. Mechanical properties such as tensile strength, hardness, fracture toughness and wear resistance are important for structural applications. Fabrication methods such as sol–gel processing, gas phase condensation, high-energy mechanical milling, chemical precipitation, plasma synthesis, etc., are used to synthesize nanoparticles but have not been successful in consolidating them. Consolidation of nanoparticles into near-net shape structures and/or bulk engineering components with nano-sized grains is difficult because of the low compressibility, high inter-particle friction and tendency for particle growth during consolidation. Different consolidation processes, viz. hot isostatic pressing, transformation assisted consolidation, microwave sintering, equal channel angular pressing, gel casting, sol infiltration, cold die pressing, etc., are being adopted to fabricate bulk nanocrystalline structures [1,2]. Rapid solidification techniques, viz. direct laser deposition, spray forming, melt infiltration, spark plasma sintering, plasma spraying, etc., that have the potential of arresting grain growth efficiently, have demonstrated significant promise in achieving nanostructures in bulk components [3,4]. In the present work, an effort has been made to fabricate a HfC reinforced tungsten metal matrix nanocomposite as proof-of-concept for making bulk component prototypes. Because of its high melting point, tungsten metal matrix composites have been applied, most particularly, for their favorable thermo-mechanical attributes. One noticeable drawback in the W matrix, however, is a reduction in material strength in the high-temperature regime. The strength of W decreases up to 80% at 1000 °C compared to that at room temperature [5]. In some composites, the tungsten matrix has been reinforced with oxides and carbides in successful attempts to further strengthen the thermal resilience of the resulting composite [6,7]. Among these, HfC has the highest thermodynamic stability and melting point and has been used especially in applications requiring thermal shielding in wear resistant environments [8–10]. In addition,

* Corresponding author at: AMPAC, Department of Mechanical, Materials, and Aerospace Engineering (MMAE), Nanoscience and Technology Center, University of Central Florida, Eng. 381, 4000 Central Florida Blvd., Orlando, FL 32816, United States. Tel.: +1 407 882 1119; fax: +1 407 882 1462.

E-mail address: sseal@mail.ucf.edu (S. Seal).

0921-5093/$ – see front matter. Published by Elsevier B.V.
doi:10.1016/j.msea.2007.05.063

due to its interstitial carbide bonding structure, HfC shares physical properties of ceramics and the electronic properties of metals forming primarily ordered non-stoichiometric phases [10]. An extensive comparative high-temperature strength study conducted by Raffo and Klopp (1963) determined that small additions of hafnium (amongst tantalum, niobium, rhenium, and carbon) in tungsten arc-melted alloys produced a dramatic increase in the high-temperature tensile strength [11]. HfC addition to the W matrix has led to reduction in grain boundary diffusion at high-temperature and acts as a particle strengthener by impeding dislocation motion.

Through processes that will be mentioned, the retention of nanostructures will be explored and the hardness and elastic modulus of the reinforced bulk component will be obtained through indentation measurements. This research has explored and characterized a vacuum plasma formed tungsten alloy that has been reinforced with a homogenous dispersion of nanoscale HfC with implications for the fabrication of bulk nanocomposites.

2. Experimental procedure

2.1. Materials

The starting powders used in the plasma forming of the bulk component were a mixture of tungsten powder (1.3 μm average particle diameters) with a reinforcement of approximately 30 nm HfC nanoparticles. The first sample created for experimentation was tungsten without any HfC particulate reinforcement (spray dried), the second and third samples were nanocomposites with the inclusion of 1.3 wt.% HfC nanoparticles in the tungsten matrix. The difference between the second and third sample was that sample 2 was blended while sample 3 was spray dried before thermal spraying. In order to improve the density of sprayed bulk components after thermal spraying, both samples 2 and 3 were subjected to hot isostatic pressing (HIP) at 1800 °C at a pressure of 205 MPa for 4 h. Spray drying [12] was carried out using a Niro Mobile Minor spray drier (Niro A/S, Denmark). Processing details and composition of the samples fabricated are tabulated in Table 1.

2.2. Vacuum plasma spraying

A 25 mm (1 in.) diameter carbon (graphite) mandrel was selected as the substrate for plasma spraying in vacuum. The CTE values for the mandrel is: $0.2 \times 10^{-5} {}^{\circ}C^{-1}$ and that of the VPS deposit: $0.4 \times 10^{-5} {}^{\circ}C^{-1}$. The powders were sprayed inside a cylindrical (diameter 1524 mm (60 in.)) water cooled vacuum chamber using a Sulzer Metco (Westbury, New York) 03C series plasma gun mounted on a robotic arm. The carbon mandrel was easily removed from the free form part due to the coefficient of thermal expansion difference between the substrate and the deposit The plasma spraying parameters used to produce the spray formed components are listed in Table 2. To further densify the microstructure and reduce porosity, samples 2 and 3 were subsequently hot isostatically pressed at 1800 °C for 4 h at a pressure of 205 MPa as listed in Table 1.

Table 2
Vacuum plasma spray parameters used for the fabrication of bulk nanostructures

Plasma gases	Ar—primary, H_2—secondary
Gun power (kW)	80–105
Argon flow rate (s.l.m.)	117
Hydrogen flow rate (s.l.m.)	21–26
Chamber pressure (Torr)	75–150
Robot motion parameters	Torch at 5000 mm/min, part at 40 rpm

2.3. SEM/FIB analysis

A JEOL 4600 scanning electron microscope (SEM) was used (acceleration voltage of 5 kV) to obtain images of the particles before and after spray drying and blending. Focused ion beam (FIB) equipment (Model FEI 200, FEI company, Hillsboro, OR) that included a magnum column workstation with a gallium ion beam was used to produce samples for the transmission electron microscopic investigation of the bulk components. The samples were thinned to thicknesses of approximately 50 nm for electron transparency. After thinning and cutting, the samples were removed using a micromanipulator and placed on a carbon TEM grid as described in a previous publication [13]. A field emission transmission electron microscope (TEM) (Model Tecnai F30, FEI company, Hillsboro, OR) was used for the investigation to ascertain the size and location of HfC particles within the as-sprayed bulk components at an acceleration voltage of 300 keV and an extraction voltage between 4.3 and 4.4 keV. Compositional analysis of HfC in the tungsten matrix was studied using a Secondary Ion Mass Spectrometer (Model ADEPT 1010, Physical Electronics Inc., Chanhassen, MN). The equipment was operated with a 3 keV cesium beam at 60° off of the specimen normal.

2.4. Nanoindentation

A nanoindenter (Nanotest 600, Micromaterials Limited, Wrexham, UK) was used to indent the specimens. A nominally sharp diamond Berkovich indenter used at a loading rate

Table 1
Matrix of powder feedstock materials used during vacuum plasma spray forming and post-spray heat treatment specification

Sample number	Composition	Feedstock agglomeration	Heat treatment[a]
1	W (1.3 μm)	Spray dried	N/A
2	W (1.3 μm) + 1.3 wt.% HfC	Blended	HIPed 4 h 1800 °C and 205 MPa
3	W (1.3 μm) + 1.3 wt.% HfC	Spray dried	HIPed 4 h 1800 °C and 205 MPa

[a] Heat treatment done after plasma spray.

of 4 mN/s up to a maximum load of 200 mN was used to determine the hardness of the specimens [14]. A 2.8 mm diameter diamond spherical indenter used at a loading rate of 50 mN/s up to a maximum load of 1 N was used to determine the elastic modulus [15].

3. Results and discussion

3.1. Powder characteristics

Spherical powders have a lower inter-particle friction coefficient, facilitating their flow through the torch for a given carrier gas flow [18]. Spray drying was used as a mechanism of feedstock (starting powder material) preparation in this study because (1) it prevented the feedstock from clogging the powder feeding assembly and halting production, (2) it is nearly impossible to entrain nanoscaled particles in the plasma stream without evaporation [19], and (3) the spray dried product was spherical, dense, and free-flowing. To enable adequate flow of particles during the plasma spray process, particular attention was paid to the feedstock powders' morphology, composition, size distribution, and density which play important roles in the quality of the bulk part (or coating) [20,21]. The particle morphology before and after the spray process were investigated using SEM. The blended 1.3 μm W–1.3 wt.% HfC powders exhibit a pasty surface structure (Fig. 1), which may pose a problem in terms of flowing through the plasma torch.

The spray dried agglomerated powder (Fig. 2) exhibits a relatively larger agglomerate size via the attractive van der Waals and polymeric binding forces overcoming the smaller dispersive electrical forces that act on the particles in suspension and during the spray drying process [22]. As the smaller particles are bound in a spheroidal shape with relatively larger tungsten particles, this powder is more suitable in a vacuum plasma forming system for bulk component manufacturing [23]. The spheroidal shape of the feedstock powders will also provide for a higher packing density during the deposition process [13]. It has also been shown that spray dried powders have higher deposition efficiencies with a higher level of predictability based on plasma spraying parameters as opposed to ground or ball-milled micron-sized powders [24].

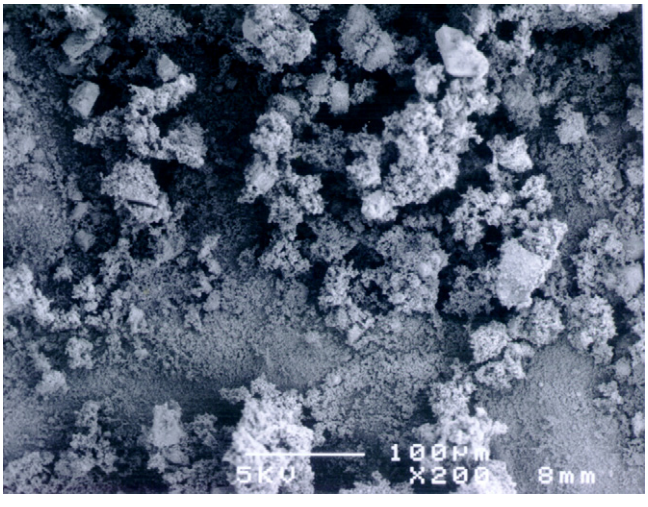

Fig. 1. SEM image of blended W–1.3 wt.% HfC nanoparticles used as a feedstock for vacuum plasma spraying.

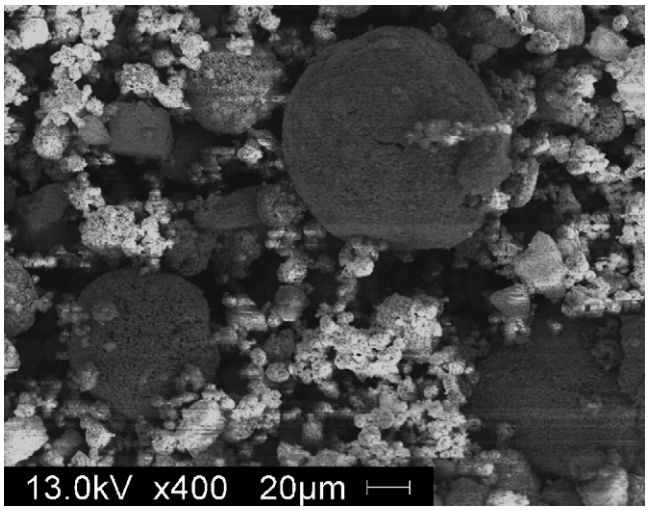

Fig. 2. SEM image of spray dried W–1.3 wt.% HfC nanoparticles used as a feedstock for vacuum plasma spraying.

3.2. Relationship between microstructure and bulk composite properties

3.2.1. Mechanical properties

Instrumented nanoindentation has previously been used to assess mechanical properties [16,17]. Elastic modulus for each of the samples is listed in Table 3 (the scatter being attributed to heterogeneous porosity). Sample 3 has a modulus close to double that of sample 1 (223 GPa versus 126 GPa). It is expected that the increase in elastic modulus of the nanocomposite is clearly due to the dispersed HfC addition given their high stiffness and the load bearing dynamics of the second phase particles in the matrix. The hardness data also presents a similar trend which can be attributed to the HfC particles. Hot isostatic pressing is also a contributing factor given the gains expected in densification and the associated reduction in porosity. Fig. 3 shows several examples of spray formed large scale W–HfC nanocomponents produced by vacuum plasma spray forming for the first time in this class of nanocomposites. The high standard deviation is attibuted to porosity which is typical for this processing technique and depending on the location of the nanoindentor the values vary.

It is to be noted that some of the HfC particles are lost during flight in the plasma torch. Since the HfC particles are encapsulated during spraying, there is considerably less loss of these

Table 3
Mechanical properties of the bulk nano W–HfC composites

Mechanical properties	Sample 1	Sample 2	Sample 3
Elastic modulus (GPa), mean	126	153	223
Standard deviation	73	34	85
Hardness (GPa), mean	4.2	4.9	5.4
Standard deviation	0.55	0.51	0.71

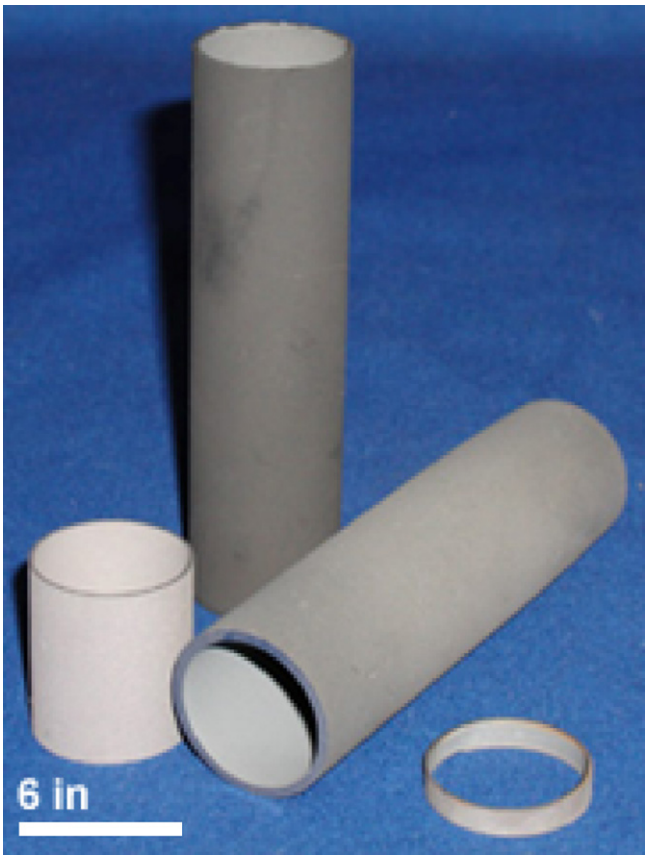

Fig. 3. W–HfC bulk nanostructured components fabricated using the plasma spray parameters listed in Table 2.

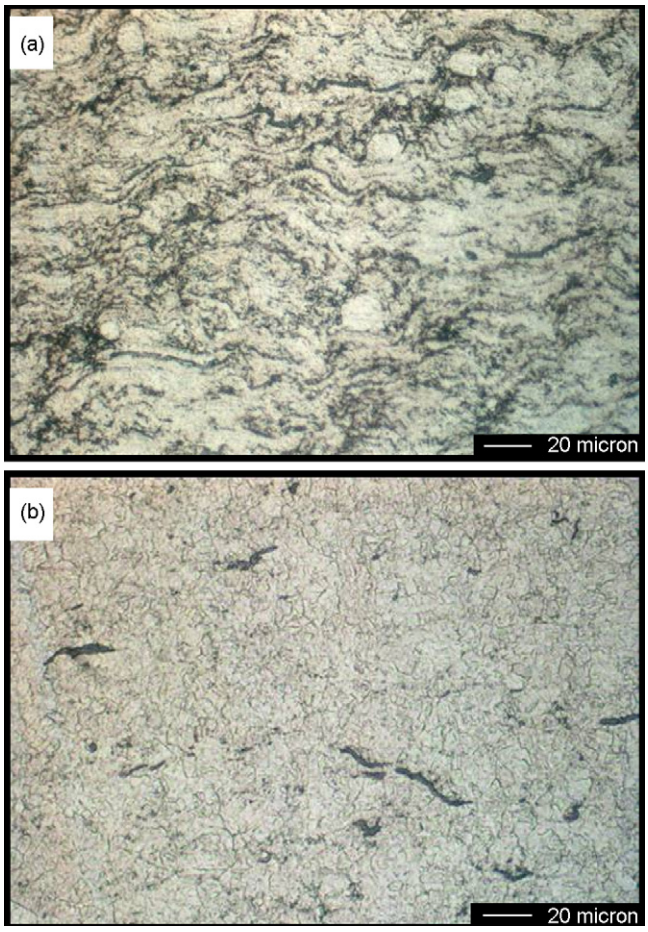

Fig. 4. Bright field optical microscopic images of W–1.3 wt.% HfC bulk component (a) prior to and (b) after hot isostatic pressing at 1800 °C and 205 MPa for 4 h.

nanoparticles as compared to the blended samples. Blended samples have shown experimental e-moduli values similar to pure tungsten and hence it is concluded that during thermal spraying, simply blending the nanoparticles with the tungsten matrix is inadequate.

3.2.2. *Microstructure and strengthening mechanisms*

Fig. 4 reveals the partial recrystallization of the plasma spray splat morphology achieved through hot isostatic pressing. Hot isostatic pressing at the selected temperature and pressure did not show any noticeable signs of grain growth or unpinning of the nano HfC reinforcing structures as observed in the TEM pictures. TEM samples of 150 nm thickness were prepared using FIB liftout as shown (Fig. 5). Sample 2 exhibits ultra-fine nanostructures of HfC at the interface regions. There were bending lattice fringes and stressed dense structures due to the coefficient of thermal expansion (CTE) differences of the particles and the matrix, thus creating dislocations which can increase hardness. The visible contrast fringes indicate the presence of back stresses built up in the matrix that would tend to oppose the motion of additional dislocations and increase the strength of the material with an increase in the number of grain boundaries (see Fig. 6) [25]. Selective area diffraction confirms the presence of both nano and micron-size grains. There was a fine distribution of visible structures within the grains, with grain sizes lower than 50 nm (Fig. 7).

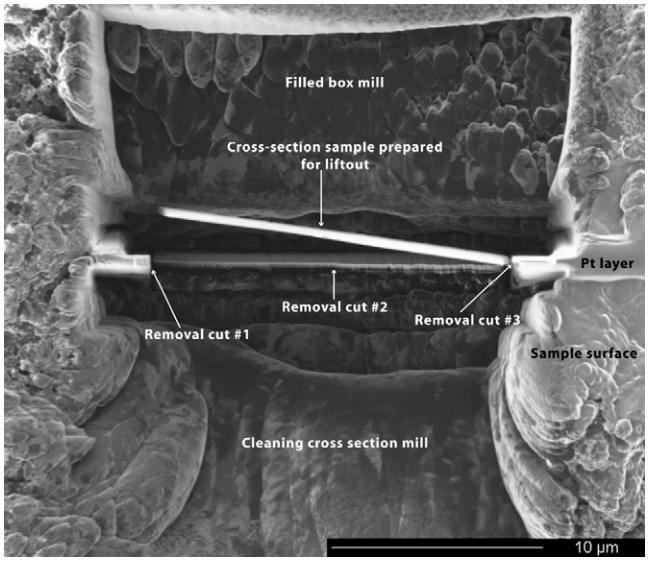

Fig. 5. Focused ion beam liftout image of the sample gathered from secondary ion imaging. The sample was subsequently used for TEM imaging.

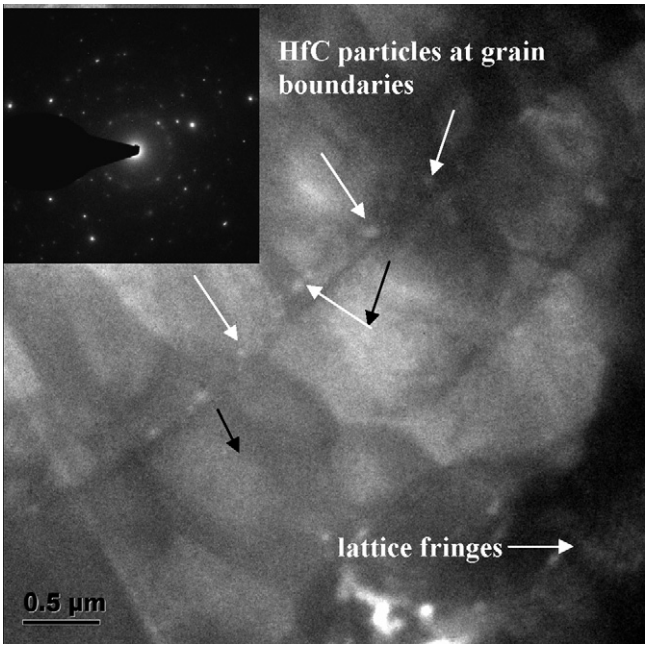

Fig. 6. High resolution transmission electron microscopy (HRTEM) of the bulk component. SAD pattern revealing the crystallinity after rapid solidification.

During plasma spray forming, particles attain the molten state and are subjected to rapid solidification with an effective cooling rate on the order of 10^6 to 10^7 K s^{-1} as opposed to the highest cooling rates of less than 10^2 K s^{-1} provided by conventional ingot solidification [28]. As a result, there is a refinement in the W microstructure, where the average W grain size is 200–500 nm (despite the starting grain size of 1.3 μm).

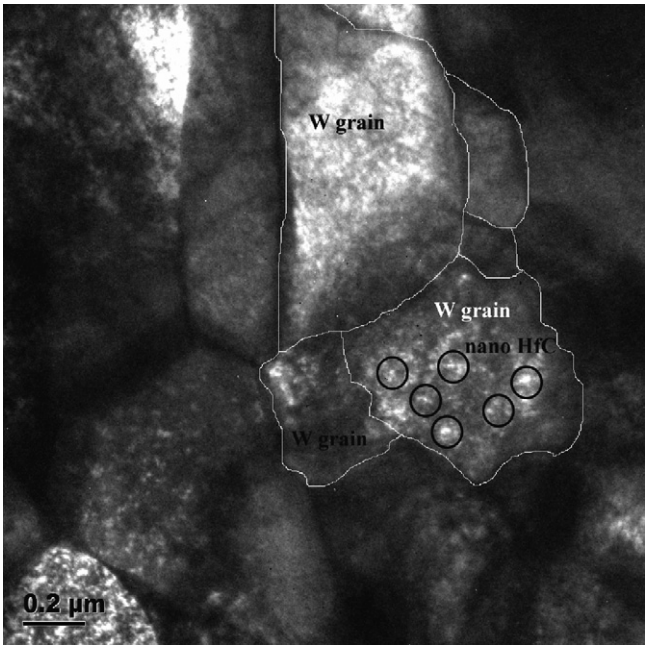

Fig. 7. HRTEM image of bulk sample cross-section formed from W–1.3 wt.% HfC powder with the distribution of nanosize particles throughout W grains (after HIPing).

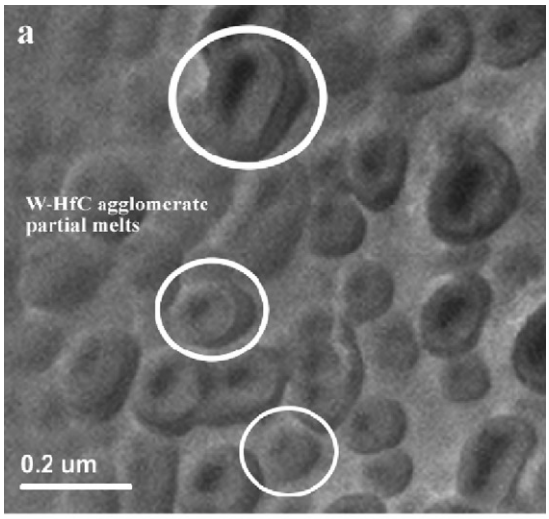

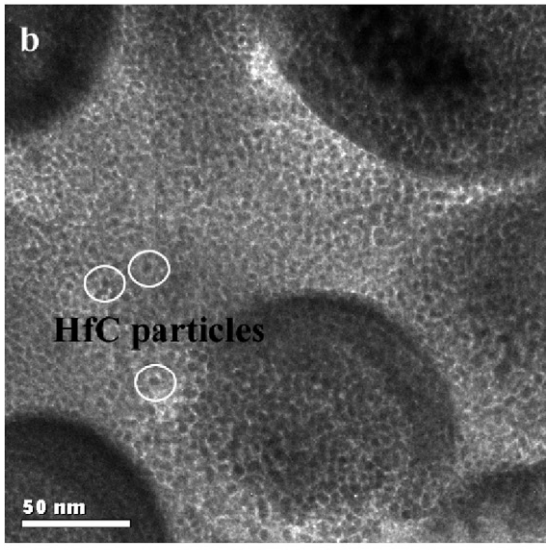

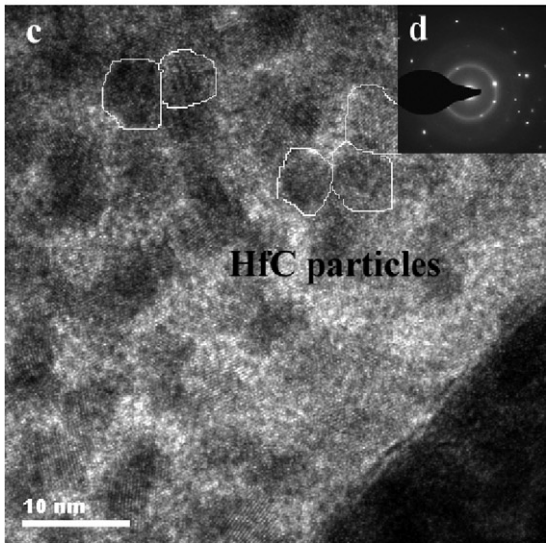

Fig. 8. High-resolution transmission electron microscopic image of nanometer-scale and homogenous grain arrangements of sample formed from W–1.3 wt.% HfC spray dried powder. The inset (d) SAED pattern shows several reflections of grains with a ring diffraction pattern.

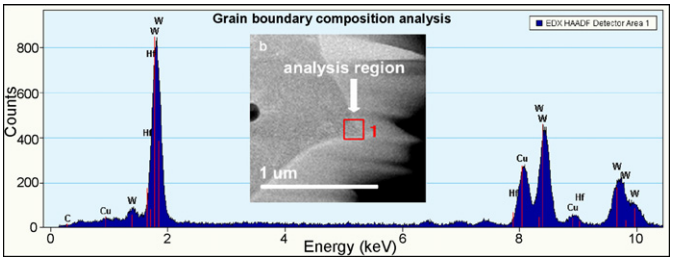

Fig. 9. EDX HAADF qualitative and quantitative compositional analysis (a) near the grain interface (analysis of area inside of square box of inset image) (b) of the bulk component formed from W–1.3 wt.% HfC spray dried powder.

Sample 3 revealed nanostructures with a HfC grain size of less than 10 nm in comparison to sample 2. Grain boundaries were very well defined and distinct (Fig. 8a). At higher magnifications, smaller reinforcing particles were found uniformly distributed throughout the larger grains (see Fig. 8b and c). Nucleation is preferred to proceed at the grain boundaries as this comprises the additional interfaces required for nucleation. Furthermore, at the rapid solidification and super cooling rates present in the plasma spray atomization and deposition environment, nucleation is also known to occur within the grain boundaries themselves [14]. Intergranular nucleation was seen within these components and during characterization of a rapidly solidified Al–Si hypereutectic near-net shape component formed in related studies [21]. Nano-sized HfC was found along the grain boundary (Fig. 9) in sample 3.

The spray dry agglomeration of the feedstock powder had some unique effects on the microstructure of the final as-sprayed bulk component. Based on a larger mean particle size of the feedstock encasing the nano-reinforcement material, the HfC was able to reach a melted or at least semi-solid state prior to deposition and resolidification as seen in Fig. 8a. Otherwise, the smaller particles do not reach the critical mass needed to enter the hot zone of the plasma flame, resulting in poor coating efficiency (and bond strength) [26]. The resulting density of the part is directly related to the density and size distribution of the inbound agglomerate and the plasma spraying parameters for spraying and deposition [24]. The presence of HfC particles in the path of dislocation motion provides obstacles to its motion and increases the amount of energy (stress) needed to pull a line of solute atoms from the dislocation line [25]. Within the tungsten matrix, strain hardening occurs through the creation of jogs at the intersection of dislocations. As the jogs become mobile, vacancies are created that act to impede further dislocation motion [27]. Presuming few or no alloying elements present and the number of vacancies increasing with continued application of stress and increasing temperature, the edge segments of the dislocation networks begin to climb and reduce the rate of work hardening. The addition of these HfC strengtheners is thought to correct for this “dynamic recovery” environment and yield increased high-temperature strength [27].

Fig. 10 shows the results from the secondary ion mass spectroscopy (SIMS) to identify and successfully describe the presence of HfC particles uniformly dispersed within the matrix (sample 3) on both the convex and concave sides of the sample

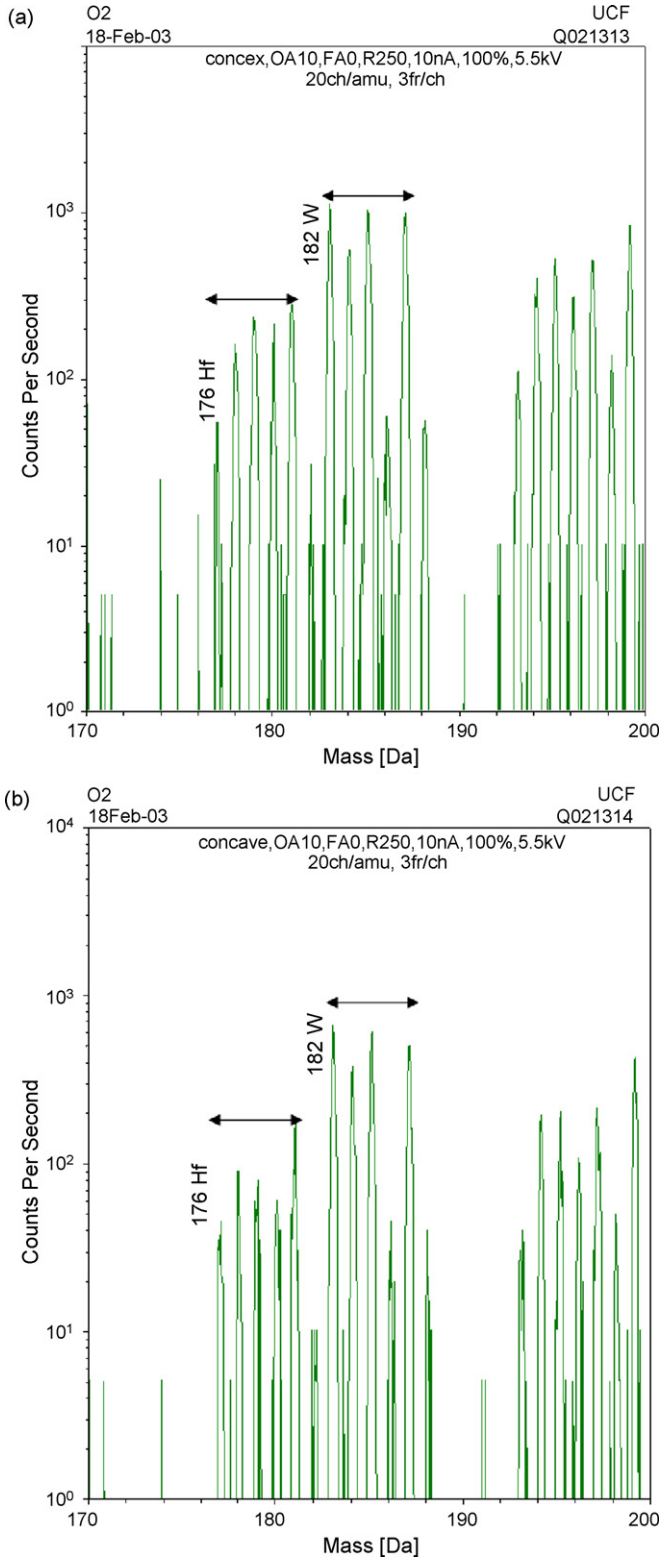

Fig. 10. Secondary ion mass spectrometry showing the uniform distribution of HfC for (a) the convex side and (b) the concave side of the nanocomposite fabricated from spray dried powder.

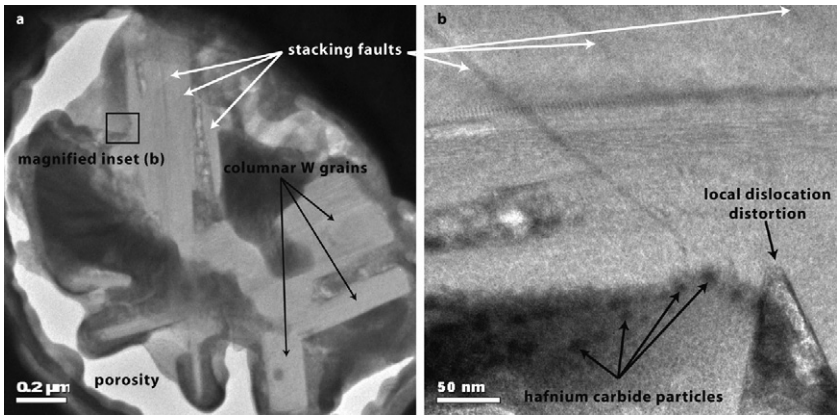

Fig. 11. (a) Transmission electron microscopic overview of sample VPS formed from W–HfC nanocomposite and (b) presence of HfC particles creating localized dislocation distortion and thereby strengthening the nanocomposite.

prepared as shown in Fig. 3. An investigation by Clark [28] of an electron beam melted W–Hf alloy showed the retention of Hf in the final ingot to be rather low. The addition of C to the W–Hf system was proposed to retain a higher concentration of the Hf in solution [5], as was also seen from our SIMS analysis in Fig. 10. However, this investigation differs from the findings of the elevated temperature properties of previous studies conducted by Raffo and Klopp [16] where we attribute the strengthening to arise from a precipitate-hardening (i.e., that of the carbide, either HfC or a W–HfC complex) mechanism rather than a solution strengthening mechanism. To further distinguish between these two different strengthening mechanisms, the effect of solid solution alloys generally becomes negligible at a temperature above half the absolute temperature of the melting point of the parent matrix metal, in which case the strengthening mechanism would be one of another nature (i.e., dispersion–strengthening or precipitation–hardening).

As a result of the high thermodynamic stability and melting point of HfC, the annealing response of W–HfC and W–Re–HfC is observed to be slow [29]. Further, because of the low free energy of formation of HfC (much lower than other carbides including WC), this W composite containing Hf and C can be presumed to be predominantly HfC [27]. Utilizing the size of the HfC particles, feedstock agglomeration, and the disintegration and rapid solidification effects of plasma spray forming, the particles were homogenously distributed and spaced throughout the matrix.

Fig. 11a reveals stacking faults within the matrix of tungsten and columnar tungsten grains while Fig. 11b reveals that the HfC particles are creating localized distortion of the dislocations leading to the strengthening of the nanocomposite. Fig. 11 also shows the existence of stacking faults and associated strain effects, which would also explain the existence of the striped contrast patterns visible in the bottom right portion of Fig. 6 [30].

4. Conclusions

The nanoscale HfC reinforcement noticeably increased the elastic modulus and hardness of vacuum plasma spray formed bulk nanocomponents. The carbide was found to lie in and around the grain boundaries, which would tend to impede dislocation motion by pinning grain boundaries and subsequently increasing the strength. VPS forming combined with hot isostatic pressing (HIP) increased the density (∼99%) and the mechanical properties. Increase in the elastic modulus and the hardness was caused by defect structures, high density, and the presence of reinforcing carbide strengthening throughout grain boundaries. Spray drying of the powder feedstock was found to have a direct effect on the density and the corresponding resultant nanostructure retention in the spray formed composites. Thus, it has been shown that Vacuum Plasma Spray is an effective tool for development of bulk metal matrix composites with improved hardness and elastic modulus.

Acknowledgements

The authors wish to thank the DOE SBIR Ph I and II, and the National Science Foundation (REU Site: EEC 0139614) and Office of Naval Research Young Investigator Award (ONR YIP - N000140210591) for their financial support. For research partnership, collaboration, time, and equipment, the authors would like to thank Plasma Processes, Inc. We also appreciate the Secondary Ion Mass Spectrometry provided by Mikhail Klimov at the Materials Characterization Facility at the University of Central Florida.

References

[1] S. Seal, S.C. Kuiry, P. Georgieva, A. Agarwal, MRS Bull. 29 (2004) 16–21.
[2] B.J. Mac Donald, M.S.J. Hashmi, J. Mater. Process Technol. 120 (1–3) (2002) 341–347.
[3] E.J. Lavernia, Q.J. Xu, Jpn. Inst. Light Met. 50 (2000) 479–485.
[4] R.B. Dandliker, R.D. Conner, W.L. Johnson, J. Mater. Res. 13 (1998) 2896–2901.
[5] S. Yih, C. Wang, Tungsten: Sources, Metallurgy, Properties and Applications, Plenum Publishing Corporation, New York, 1978, pp. 500–515.
[6] G.M. Song, Y.J. Wang, Y. Zhou, Int. J. Refract. Met. H. 21 (2003) 1–12.
[7] P.G. Caceres, Mater. Charact. 49 (2002) 1–9.
[8] Y. Saito, T. Matsumoto, K. Nishikubo, Carbon 35 (12) (1997) 1757–1763.
[9] M. Opeka, I. Talmy, E. Wuchina, J. Zaykoski, S. Causey, J. Eur. Ceram. Soc. 19 (1999) 2405–2414.

[10] H.O. Pierson, Handbook of Refractory Carbides and Nitrides: Properties, Characteristics, Processing and Applications, Noyes Publications, New Jersey, 1996, pp. 331–334.
[11] A.C. Fischer-Cripps, Nanoindentation, Springer-Verlag, New York, 2002, pp. 265–269.
[12] E. Lavernia, Y. Wu, Spray Atomization and Deposition, John Wiley & Sons, West Sussex, 1996, pp. 627–631.
[13] A. Agarwal, T. McKechnie, Adv. Mater. Process 159 (2000) 44–46.
[14] W.C. Oliver, G.M. Pharr, J. Mater. Res. 7 (6) (1992) 1564–1583.
[15] J. Alcala, A.E. Giannakopoulos, S. Suresh, J. Mater. Res. 13 (5) (1998) 1390–1400.
[16] P. Raffo, W. Klopp, NASA Technical Memorandum TM X-52131 (1965) 1–21.
[17] S. Rajagopalan, R. Vaidyanathan, J. Miner. Met. Mater. Sci. 54 (9) (2002) 45–48.
[18] M. Boulos, Met. Powder Rep. 59 (2004) 16–21.
[19] S.L. Girshick, High Temp. Mater. Process 4 (2000) 379–384.
[20] G. Bertrand, C. Filiatre, H. Mahdjoub, A. Foissy, C. Coddet, J. Eur. Ceram. Soc. 23 (2003) 263–271.
[21] K.E. Rea, A. Agarwal, T. McKechnie, S. Seal, Microsc. Res. Technol. 66 (1) (2005) 10–17.
[22] S. Lukasiewicz, J. Am. Ceram. Soc. 72 (4) (1989) 617–624.
[23] T. Laha, A. Agarwal, T. McKechnie, K. Rea, S. Seal, Acta Mater. 53 (2005) 5429–5438.
[24] J. Li, H. Liao, X. Wang, C. Coddet, H. Chen, C. Ding, Thin Solid Films 460 (1–2) (2004) 101–115.
[25] G.E. Dieter, Mechanical Metallurgy, McGraw-Hill, Boston, 2000, pp. 31–41.
[26] X. Cao, R. Vassen, S. Schwartz, W. Jungen, F. Tietz, D. Stoever, J. Eur. Ceram. Soc. 20 (2000) 2433–2439.
[27] P. Raffo, W. Klopp, NASA Technical Memorandum TN D-3248, 1966, pp. 1–12.
[28] J.S. Clark, A.L. Mincher, G.N. Villee, Rept E. I. Du Pont de Nemours and Company, RTD-TDR 63, 1963, p. 4236.
[29] W.D. Klopp, W.R. Witzke, J. Less-Common Met. 24 (1971) 427–443.
[30] Y. Nakayama, S. Weissmann, T. Imura, Proceedings of the Technical Conference, Interscience Publishers, New York, 1962, pp. 93–95.